Prospects of temperature performance enhancement through higher resonant phonon transition designs in GaAs-based terahertz quantum-cascade lasers

Supplementary information

Aleksandar Demić,* Zoran Ikonić,† Paul Dean,‡ and Dragan Indjin§
[1] *School of Electronic and Electrical Engineering*
University of Leeds, LS2 9JT, Leeds, UK

In this supllementary document we provide an example on determining cut-off temperature of terahertz QCL device. We use density matrix model to extract material gain dependence on frequency, external electrical field bias and temperature of record temperature operation design [1].

SUPPLEMENTARY INFORMATION

Our density matrix (DM) transport model [2–4] is originally based on density matrix approach that was used for optimisation of former temperature operation record [5] that lased up to 200 K. The key improvement in our model is that is independent from number of states considered for solving Schrödinger - Poission equations and thus applicable to variety of terahertz QCL designs.

The corresponding theory on our model can be found in [3, 4, 6]; in [3] we laid out in detail how we extract output data (current density, material gain and optical power) and also pinpointed some shortcomings of the model in terms of accurately predicting temperature dependence of threshold current.

In this paper we are applying high precision of this model in determining cut-off lasing temperature of various QCL designs. We also used this feature in our earlier work to propose a new optimized design type [7]. Works in [8, 9] are based on similar model as ours and in [8] it was also outlined that this model can be used for precise cut-off temperature prediction, while not having as precise prediction of the current density.

In the paper we provided a detailed six-part figure (Figure 1 in the paper) with several significantly different THz QCL designs where we plotted temperature dependence of the material gain that outlines our model's precision and reliability. In this supplemental file we provide additional information on how we generated these temperature dependencies.

Our algorithm can be summarized in these steps:

1. Set lattice temperature.
2. Set electrical bias value (electric field K, which correlates to terminal voltage of the device).
3. Solve Schrödinger-Poission and kinetic balance equation (under equithermal subband approximation) in self-self-consistent manner - this algorithm nests iterative algorithm for solving Schrödinger-Poission equations within minimization algorithm for determining electron temperature [10].
4. Extract current density value and material gain dependence $g(f)$ on frequency using DM transport model.
5. Set the peak of $g(f)$ as the unsaturated material gain value and the corresponding frequency point as the lasing frequency - this is a valid approximation as at this frequency the net value of gain minus loss is minimal. This approach can be further improved with the model for frequency dependence of waveguide loss (applicable mainly for single plasmon waveguides).
6. Repeat steps 3. - 5. for a full range of applied electrical bias values.

* A.Demic@leeds.ac.uk
† Z.Ikonic@leeds.ac.uk
‡ P.Dean@leeds.ac.uk
§ D.Indjin@leeds.ac.uk

7. Extract unsaturated material gain dependence on bias. $g(f_{\max}, K)$ and current density dependence on bias $J(K)$. The peak of $g(f_{\max}, K)$ should correspond to resonant tunnelling, this can be verified through wavefunction and energy inspection, while the peak of $J(K)$ corresponds the case when device exhibits negative differential resistance (NDR), in the experiment this typically causes abrupt stopping of lasing (optical power). Declare the corresponding bias value K_{NDR} where the peak of $J(K)$ occurs.

8. Declare peak of $g_{\max} = g(f_{\max}, K_{\max})$ as the highest unsaturated material gain at temperature set in step 1.

9. Declare gain at K_{NDR} as unsaturated material gain at temperature set in step 1. where the device is likely to exhibit NDR, $g_{\mathrm{NDR}} = g(f_{\max}, K_{\mathrm{NDR}})$.

10. Repeat steps 6. - 8. for range of lattice temperature values.

11. Extract unsaturated material gain on temperature $g(T) = g(f_{\max,K_{\max},T})$ and the NDR gain $g_{\mathrm{NDR}}(T) = g(f_{\max,K_{\mathrm{NDR}},T})$.

12. Determine design's cut off temperature as the value where either $g(T)$ or $g_{\mathrm{NDR}}(T)$ decays up to the value of estimated waveguide losses. Since K_{NDR} is always lower or equal than $K_{\max}$, using $g_{\mathrm{NDR}}(T)$ would impose the stricter cut off condition and likely correlate to realistic experiment measurement.

Note that in the paper we used $g_{\mathrm{NDR}}(T)$ for all analysed devices, and we outlined the importance of this approach in our earlier work [7]. In most cases $K_{\max}$ is equal to K_{NDR}, however it would be unsafe to use $g_{\max}(T)$ in the optimisation procedure, as we are varying multiple QCL layers and among them there may be "exotic" designs that exhibit majority of their lasing in NDR which from experimental experience is rare.

We will now illustrate procedure by applying this algorithm to the record temperature operation THz QCL design [1].

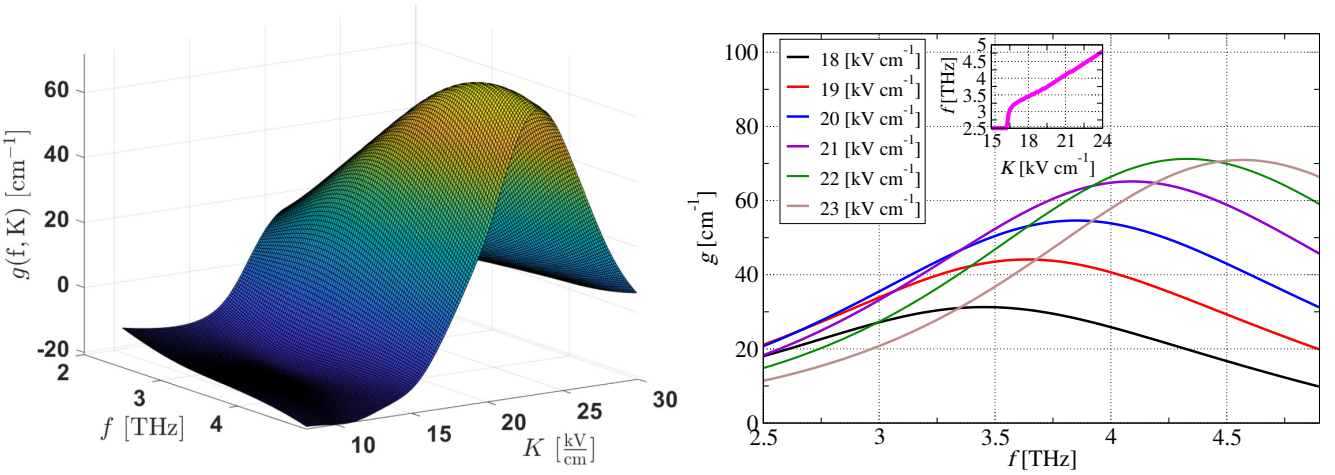

(a) $g(f, K, T = 5\ \mathrm{K})$

(b) $g(f, K \in [18, 23]\ \frac{\mathrm{kV}}{\mathrm{cm}}, T = 5\ \mathrm{K})$

FIG. 1. Material gain dependence on frequency and applied bias of 250 K temperature record THz QCL structure [1] at lattice temperature of 5K in a) three dimension representation and b) multiple trace representation (traces of particular material gain dependence on frequency for the electric bias K in range of $K \in [18, 23]\ \frac{\mathrm{kV}}{\mathrm{cm}}$). Inset in the figure on the right illustrates peaks of material gain at particular bias points (peaks of traces in the figure on the right). This inset illustrates Stark effect and displays most probable lasing frequency of the device.

In Fig. 1 we illustrate step 6. of our approach on exemplary structure [1] at lattice temperature of 5K. The graph in Fig. 1a) illustrates three dimensional representation of material gain profile $g(f, K)$ while figure 1b) on the right offers an informative description on underlying Physics. We can safely assume that the lasing mode will correspond to the peak of $g(f, K)$ at each bias point which allows us to implement step 7. and extract material gain dependence on bias. We can also witness the Stark effect as the traces in Fig. 1b) shift toward the higher frequency as the bias is increased. Inset in Fig. 1b) illustrates that lasing frequency of this design would be around 4 THz, which is in an excellent agreement with the experiment in [1].

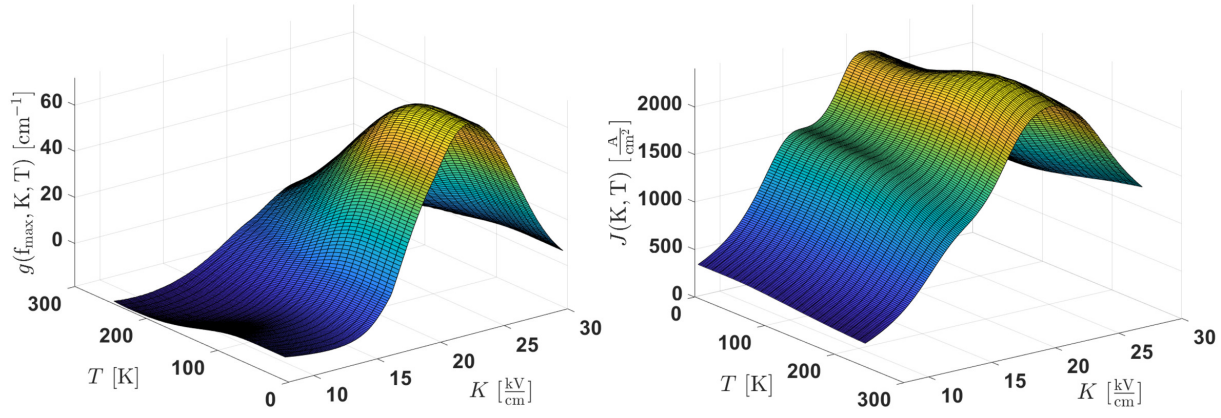

(a) $g(f_{\max}, K, T)$ (b) $J(K, T)$

FIG. 2. a) Material gain dependence on temperature and applied bias of 250 K temperature record THz QCL structure [1]. Gain values were taken at the peaks of frequency dependence of material gain at each bias point. b) Current density dependence on temperature and applied bias of 250 K temperature record THz QCL structure [1].

As we can extract material gain $g(f_{\max}, K)$ and the current density $J(K)$ dependence on bias at particular lattice temperature, we are able to repeat this step for range of temperature values. In Fig. 2 we illustrate step 7. of our approach on exemplary structure [1]. The material gain is, as expected, the largest at 5 K and decays towards the higher temperatures, while the current density has rising and saturating profile with the temperature. We can also notice a formation of two pronounced humps at low temperature where the lower one disappears at higher temperature. This agrees very well with the experimental $I-V$ measurements and illustrates underlying Physics of resonant phonon design. The formation of this hump occurs at bias that corresponds to case when QCL is such voltage that lower lasing level (LLL) is at the resonance with the injection level (ILL) from the previous QCL period. This naturally occurs before desired alignment between ILL and upper lasing level (ULL). At low temperature LO-phonon process is not dominant, thus alignment of ILL and LLL will cause efficient pumping of LLL if the injection barrier is not thick/high enough. In many LO-phonon designs this can be experimentally verified as well and the effect typically shows $I-V$ dependencies with a "hump" at low temperature that disappears at high temperature. The hump disappearance is attributed to the efficiency of LO-phonon scattering mechanism, even though ILL and ULL are undergoing resonant tunelling, this is not as efficient as extraction of LLL level via LO-phonon scattering within its own QCL period. Note that this effect is also affected by the overlap of LLL and ILL within the same QCL period and injection barrier thickness/height.

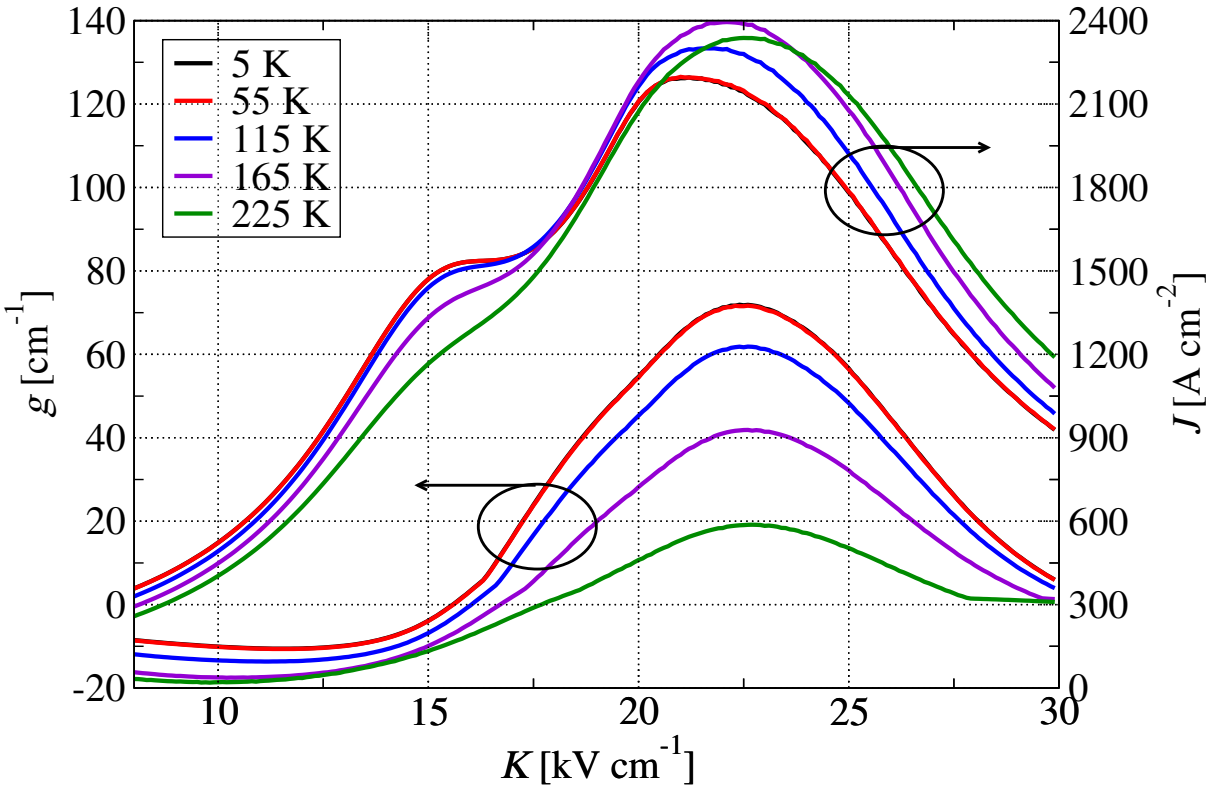

FIG. 3. Material gain and current density dependence on electrical bias at different temperatures. This graph represents multiple trace representation of graphs presented in Figure 2.

Figure 3 represents current density and material gain dependence on bias at different lattice temperatures. This figure is multiple trace representation of three dimensional graphs in Fig. 2. We can directly use Fig. 3 for data fitting to the experimental measurement. This is what we did in our previous work in [3] for a different QCL design. We can see in Fig. 3 that the current density peaks are in good agreement with the experimentally measured values in [1] where measured peaks were around 2500 $\frac{\text{A}}{\text{cm}^2}$. Existing mismatch of around 100 – 150 $\frac{\text{A}}{\text{cm}^2}$ between calculated and measured current peaks before NDR, can be attributed to the robustness of the model [8], the fact that we haven't fitted interface roughness scattering parameters (model predicts cut off temperature well despite this, because this effect is negligible at high temperatures), and also to experimental fluctuations during growth (i.e with doping density value). The material gain demonstrates a peak around 22.5 $\frac{\text{kV}}{\text{cm}}$ at all temperatures, however current density exhibits NDR in slightly different bias values at some temperatures, and we took this into account in the paper.

Since we have temperature profiles of material gain on bias and temperature we can then easily extract peak gain dependence on temperature (step 12.) and estimate the cut-off temperature of QCL designs. In the paper we applied this algorithm for variety of known designs and used it for device optimisation.

[1] A. Khalatpour, A. K. Paulsen, C. Deimert, Z. R. Wasilewski, and Q. Hu, "High-power portable terahertz laser systems," *Nature Photonics*, vol. 15, no. 1, pp. 16–20, 2021.

[2] T. V. Dinh, A. Valavanis, L. J. M. Lever, Z. Ikonić, and R. W. Kelsall, "Extended density-matrix model applied to silicon-based terahertz quantum cascade lasers," *Phys. Rev. B*, vol. 85, no. 23, p. 235427, 2012.

[3] A. Demić, A. Grier, Z. Ikonić, A. Valavanis, C. A. Evans, R. Mohandas, L. Li, E. H. Linfield, A. G. Davies, and D. Indjin, "Infinite-period density-matrix model for terahertz-frequency quantum cascade lasers," *IEEE Transactions on Terahertz Science and Technology*, vol. 7, no. 4, pp. 368–377, 2017.

[4] A. Demić, Z. Ikonić, R. W. Kelsall, and D. Indjin, "Density matrix superoperator for periodic quantum systems and its application to quantum cascade laser structures," *AIP Advances*, vol. 9, no. 9, p. 095019, 2019.

[5] S. Fathololoumi, E. Dupont, C. W. I. Chan, Z. R. Wasilewski, S. R. Laframboise, D. Ban, A. Mátyás, C. Jirauschek, Q. Hu, and H. C. Liu, "Terahertz quantum cascade lasers operating up to $\sim$ 200 K with optimized oscillator strength and improved injection tunneling," *Opt. Express*, vol. 20, no. 4, pp. 3866–3876, 2012.

[6] A. Demić, *Density Matrix Modelling of Terahertz Frequency Quantum Cascade Lasers: Steady State Analysis and Maxwell-Bloch Dynamics*. PhD thesis, University of Leeds, 2020, `http://http://etheses.whiterose.ac.uk/26539/`.

[7] A. Demić, Z. Ikonić, P. Dean, and D. Indjin, "Dual resonance phonon–photon–phonon terahertz quantum-cascade laser: physics of the electron transport and temperature performance optimization," *Optics Express*, vol. 28, no. 26, pp. 38788–38812, 2020.

[8] B. A. Burnett, A. Pan, C. O. Chui, and B. S. Williams, "Robust density matrix simulation of terahertz quantum cascade lasers," *IEEE Transactions on Terahertz Science and Technology*, vol. 8, no. 5, pp. 492–501, 2018.

[9] B. A. Burnett and B. S. Williams, "Density matrix model for polarons in a terahertz quantum dot cascade laser," *Phys. Rev. B*, vol. 90, no. 15, p. 155309, 2014.

[10] V. D. Jovanović, D. Indjin, N. Vukmirović, Z. Ikonić, P. Harrison, E. H. Linfield, H. Page, X. Marcadet, C. Sirtori, C. Worrall, H. E. Beere, and D. A. Ritchie, "Mechanisms of dynamic range limitations in GaAs/AlGaAs quantum-cascade lasers: Influence of injector doping," *Appl. Phys. Lett.*, vol. 86, no. 21, p. 211117, 2005.